Journal of Power Sources 663 (2026) 238924

Contents lists available at ScienceDirect

Journal of Power Sources

journal homepage: www.elsevier.com/locate/jpowsour

Impact of carbon black distribution on dry coating and PTFE-fibrillation in cathodes for lithium-ion batteries

Serkan Z. Damnali [a,b,c,*], Benjamin Villard [a], Matthias Leeb [d], Berkant Tekin [a], Thomas Woehrle [a], Ruediger Daub [d,e], Alice Hoffmann [c], Markus Hoelzle [c]

[a] BMW AG, Battery Cell Competence Center, Lemgostraße 7, 80935, München, Germany
[b] Ulm University, D-89081, Ulm, Germany
[c] ZSW – Zentrum für Sonnenenergie, und Wasserstoff-Forschung Baden-Württemberg, Lise-Meitner-Straße 24, 89081, Ulm, Germany
[d] Technical University of Munich, TUM School of Engineering and Design, Institute for Machine Tools and Industrial Management (iwb), Boltzmannstraße 15, Garching, 85748, Germany
[e] Fraunhofer Institute for Casting, Composite and Processing Technology (IGCV), Am Technologiezentrum 10, 86159, Augsburg, Germany

ARTICLE HIGHLIGHTS

- Dry coating of cathodes via calendering with PTFE binder.
- Carbon black distribution was controlled through variation of premixing times.
- Carbon black distribution affected compressibility and PTFE-fibrillation.
- Homogenous carbon black distribution facilitated calendering process.
- Homogenous carbon black distribution led to strong and uniform PTFE-fibrillation.

GRAPHICAL ABSTRACT

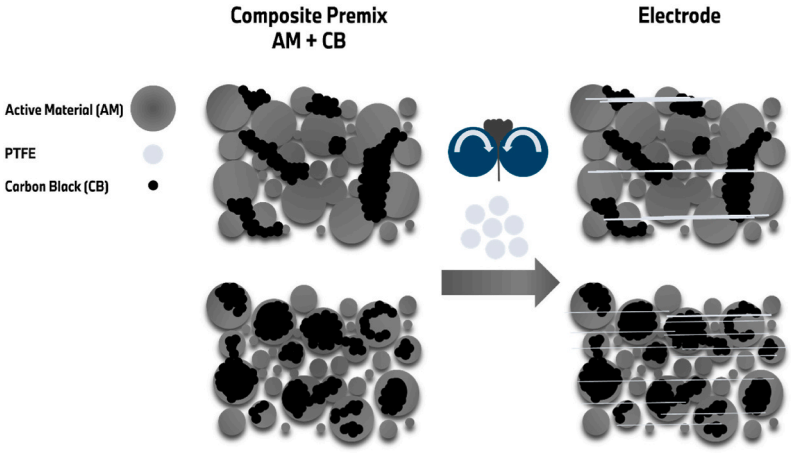

ARTICLE INFO

Keywords:
Lithium-ion battery
Dry coating
Carbon black
Distribution
PTFE
Calendering

ABSTRACT

Solvent-free technologies have gained significant attention as promising alternatives for producing lithium-ion battery electrodes. Dry electrode manufacturing by roll-to-roll calendering based on a polytetrafluoroethylene binder has reached high technological maturity, offering the potential to lower manufacturing costs and enable sustainable production. Here, the influence of carbon black distribution on the properties of the composite granules, the calendering step for dry-coated cathodes, as well as the interplay between carbon black and polytetrafluoroethylene is investigated. Various carbon black distribution patterns are obtained by varying the mixing time of the active material and carbon black during premixing. The results reveal that carbon black distribution has a critical impact on the processibility of the composite. Homogenous mixtures with uniformly

* Corresponding author. BMW AG, Battery Cell Competence Center, Lemgostraße 7, 80935, München, Germany.
E-mail address: serkan-zeki.damnali@bmw.de (S.Z. Damnali).

https://doi.org/10.1016/j.jpowsour.2025.238924
Received 3 September 2025; Received in revised form 27 October 2025; Accepted 21 November 2025
Available online 25 November 2025

distributed carbon black exhibit improved compressibility and higher degrees of polytetrafluoroethylene fibrillation in the electrodes after calendering. Both, the electronic and ionic conductivity, as well as the electrochemical performance of the electrodes, indicate that different distributions of carbon black still result in comparable characteristics of the electrodes, only if a sufficient percolation network is established. The findings contribute to the understanding of the basic interaction between carbon black and polytetrafluoroethylene in dry-coated cathodes and facilitate the design of electrode formulations tailored to specific process requirements.

1. Introduction

Solvent-free production of lithium-ion battery (LIB) electrodes has emerged as a viable alternative to the conventional wet coating process to reduce manufacturing costs of LIB cells [1–3]. Conventional wet coating involves the dissolution of the electrode binder and the dispersion of active materials and conductive additives (CA) in a solvent to form a suspension, which is then coated onto the current collector, followed by the evaporation of the solvent [4,5]. Approximately 40 % of the energy consumption in LIB fabrication is attributed to the evaporation, condensation, and redistillation of the solvent in the slurry-based process [6]. The drying process is particularly challenging for cathodes, where usually N-methyl-2-pyrrolidone (NMP) is used as the casting solvent, as drying of the coating becomes more energy intensive in comparison to water-based anodes, and the handling of NMP requires specialized safety protocols due to its toxicity [6–9]. In solvent-free electrode fabrication, both production space and energy needs are markedly reduced by the elimination of long drying sections, which reduces space requirements and manufacturing costs by 10–15 % [1,10,11]. Moreover, the omission of environmentally hazardous solvents adds to a more sustainable electrode production. The global demand for LIB cells is expected to increase significantly in the coming years due to the electrification of the mobility sector, which is a crucial element to fulfill climate targets [12,13]. The adoption of solvent-free technologies can contribute to support the transition towards affordable electromobility.

One of the most promising approaches for solvent-free electrode fabrication is the roll-to-roll dry-coating process involving direct calendering of the electrode powders blended beforehand by a dry mixing process [3,11,14]. This technology was initially developed by Maxwell Technologies Inc [15]. in 2003 for supercapacitor applications and later identified by Tesla Inc. for its potential in large-scale battery electrode production [3]. When applying this process for the fabrication of electrodes, polytetrafluoroethylene (PTFE) is used instead of polyvinylidene fluoride (PVDF) as an electrode binder, owing to its ability to form a network of interconnected fibrils when subjected to strong shear forces [14,16,17]. These fibrils ensure mechanical integrity of the electrode films by interconnecting the active material and CA. The required shear force is achieved during mixing and by controlling the differential speeds of the rollers during calendering [14]. Among other dry coating technologies, such as vapor deposition or powder spray coating, direct calendering can meet the demands of large-scale battery manufacturing, particularly in achieving high production throughput rates and maintaining homogenous mass loadings [2,3,14]. Therefore, this technology is considered as a suitable candidate to replace the conventional wet coating process [14].

However, eliminating the solvent and introducing PTFE as an electrode binder present significant challenges. High energy inputs are required during powder dry mixing to homogenously distribute the CA and the binder within the electrode composite without breaking the active material particles [3,18]. Thereby, the interaction between the binder and CA must be controlled and a sufficient PTFE fibrillation must be achieved, determining the mechanical and electrochemical electrode characteristics of the electrode [18–21].

To address these challenges, extensive research has been conducted on the influence of mixing parameters and mixing sequence on the CA distribution. While most studies have investigated the influence of the mixing procedure on the carbon black (CB) distribution for conventional wet coating process, less work was dedicated to its impact for dry coating [22,23]. Bauer et al. [24] and Bockholt et al. [25] have explored a dry premixing approach of active material and CB for slurry preparation, finding that high energy input can effectively deagglomerate the CB and facilitates the coating of the active material particles with the conductive additive. Both studies revealed that a lack of long-range electronic pathways due to strong CB deagglomeration is detrimental to the characteristics of the electrode. However, the electrochemical performance of the electrodes was enhanced by subsequently decreasing the porosity by calendering, mitigating this issue. Further research has explored the influence of the mixing sequence on the slurry characteristics and the resulting electrodes. Wang et al. [26] demonstrated that the interplay between CB and binder in the electrode is governed by the mixing parameters. Lischka et al. [27] investigated the CB deagglomeration with increasing energy input during dry mixing of active material and CB. Moreover, the authors studied the influence of the CB distribution on the powder conductivity and flowability. Lim et al. [28] compared the dispersibility of carbon nano tube (CNT)/CB blends in wet-and dry-processed electrodes and reported superior dispersibility in dry electrodes. Hence, this study did not investigate the film formation capabilities of the dry mixed composites. Yonaga et al. [29] studied the impact of CB distribution on the performance of spray-coated cathodes with PVDF binder. By varying the rotation speed of the mixer, three distinct CB distributions from large CB agglomerates to a homogenous coating of the CB around the active materials with only small agglomerates were achieved. The electrochemical characterization of the manufactured electrodes revealed a poor electrochemical performance for the electrode with the most homogenous CB distribution. This observation was explained by the evolution of high tortuous long- and short-range electronic pathways and increased charge transfer impedance by the uniform coating of the CB on the active material surface. Gao et al. [30] investigated the effects of mixing intensity and sequence on the powder flowability and the electrochemical performance of cathodes fabricated via electrostatic spray deposition with PVDF. In their study, a more homogenous CB distribution led to improved flowability of the mixed powders during the fabrication process. The best electrochemical performance was achieved when the electrode contained a mixture of both, large and small CB agglomerates, ensuring short- and long-range electronic contacts in the electrode. The existing literature on the distribution of CB in solvent-free manufactured electrodes has focused on electrodes fabricated via electrostatic static spray deposition with PVDF binder. However, the effect of the CB distribution on the mechanical and electrochemical characteristics of PTFE-based dry-coated cathodes is not well understood. Besides the work of Choi et al. [31], where superior performance of a PTFE/CB composite, which was synthesized by adding ionic surfactants to ensure a uniform distribution of the passive materials in the electrode, was demonstrated, existing research in this area has primarily focused on the PTFE fibrillation during processing [32], including the impact of active material morphology [33]. Tao et al. studied the impact of the mixing time on the degree of PTFE fibrillation in a one pot approach where all components are mixed together and the fibrillation step is varied [34]. However, it was not possible to study the carbon black distribution in this one pot approach due to the strong interaction between the PTFE and the carbon black whereby both agglomerate together during mixing. Furthermore, the effect of CBs with various properties was studied in dry coated cathodes with PTFE binder

[35,36].

Therefore, this work investigates the influence of CB distribution on the granule characteristics after mixing, the calendering step, and on the interaction between CB and PTFE in dry-coated cathodes, as well as the electronic properties and electrochemical performance of the produced cathodes. Four different powder mixtures with distinct CB distributions were generated by varying the premixing time of active material and CB. Subsequently, cathodes with industry related electrode formulations with an active material share of 97.5 wt% and an areal capacity of 3.95 mA h cm^{-2} were produced by direct calendering. The cathodes were characterized using microscopy to study the CB distribution and tensile tests were conducted with the free-standing films (FSFs), which are obtained as intermediate stages before laminating the film onto the current collector, to investigate the mechanical integrity. The electrochemical characteristics such as cycle life and rate capability were evaluated in single-layer pouch (SLP) cells. The results provide an understanding for the interaction between CB and PTFE and insights into designing dry coated cathodes with tailored CB distributions by revealing the requirements.

2. Experimental

2.1. Composite and electrode preparation

The composites and electrodes were prepared in a dry room atmosphere with a permanent dew point below −50 °C. The cathode compositions consisted of 97.5 wt% $LiNi_{0.8}Mn_{0.1}Co_{0.1}$ (NMC 811) active material with poly- and single-crystalline particles (217 mA h g^{-1} at 0.1C, Umicore, Belgium), 1.0 wt% PTFE (Chemours, USA), and 1.5 wt% of LITX®MAX90 (Cabot Corporation, USA) as conductive additive. The active material and the CB were premixed using a high shear mixer (FML10, Zeppelin, Germany) operating at 3800 rpm without temperature control. Powder samples were extracted after 2, 10, 30, and 60 min of mixing duration (further called P2, P10, P30, and P60). Further investigations with reduced PTFE contents of 0.8 wt% and 0.6 wt% were made for P2 and P60, while the CB fraction was kept at 1.5 wt% and the active material share was adjusted accordingly. After cooling of the premixed samples, PTFE was added and the mixture was blended in a tumble mixer (Turbula, Willy A. Bachofen AG, Germany) for 10 min under mild shear conditions by choosing a rotational speed of 34 rpm to achieve homogenous distribution throughout the mixture without causing fibrillation.

The blends were fed into a twin-screw extruder (Process 11, Thermo Fisher, USA) with 11 mm screw diameter at a throughput of 0.3 kg h^{-1}. The screw design involved conveying and kneading elements to impart shear force and fibrillate the PTFE. A rotational speed of 200 rpm and a temperature of 110 °C were applied by the extruder to promote PTFE fibrillation. The extruded granules (further called G2, G10, G30, and G60) were ground down into smaller flakes using a blender (Nutribullet, USA) to improve processibility of the material during calendering.

The granules were dosed over a width of 100 mm in a two-roll calendar (GK-300L, 300 mm roller diameter, Saueressig Group, Germany) with horizontally aligned rolls, which was operated in a force-controlled mode at linear loads of up to 125 N mm^{-1} and a roll speed of 0.1 m min^{-1}. Initially, a FSF was pressed from the granules. Subsequently, the desired cathode areal capacity of 3.95 mA h cm^{-2} was adjusted in multiple calendering steps, whereas the induced shear force was controlled through the relative roller speeds. Afterwards, the FSF was laminated onto a primed aluminum current collector foil with a thickness of 16 μm including a 1 μm primer coating (EnSafe91, Armor, France) using a calendar with vertically aligned rolls (CA9, Sumet Technologies GmbH & Co. KG, Germany). The calendar was operated at a roller temperature of 130 °C and a linear load of 85 N mm^{-1} to tune the electrode porosity to 25 %, corresponding to a composite density of 3.5 g cm^{-3}.

Graphite anodes were fabricated using conventional slurry coating. The anodes were composed of 95.8 wt% graphite (Zichen GT, China), 1.6 wt% carboxymethyl cellulose (CMC) (Nippon, Japan), 1.6 wt% styrene-butadiene (SBR) (Zeon Chemicals LP, Japan), and 1.0 wt% C-NERGYTM Super C65 (Imerys Graphite & Carbon, Switzerland). A binder solution was prepared by dissolving CMC in deionized water at a mass ratio of 2 % and stirring over night at 350 rpm. Then, Super C65 was added and dispensed using a centrifugal mixer (Thinky ARE 250, Japan) at a rotational speed of 1200 rpm and a mixing time of 15 min. The graphite was then added in equal quantities within two steps, with the dispersion mixed in the centrifugal mixer for 5 min at 1200 rpm after each addition. Finally, the SBR was added, and the slurry was diluted to a solid content of 47 wt%. The slurry was coated onto a copper current collector foil with a roll-to-roll coater (Mathis AG, Switzerland), with the coating parameters adjusted to target an areal capacity of 4.4 mA h cm^{-2}. After drying, the anodes were calendered (CA9, Sumet Technologies GmbH & Co. KG, Germany) at 80 °C and a linear load of 66 N mm^{-1} to a density of 1.6 g cm^{-3}.

2.2. Composite and electrode characterization

The distribution of CB and its interaction with PTFE were characterized using scanning electron microscopy (SEM) imaging of the mixed powders and respective electrodes. The SEM analyses were performed at an acceleration voltage of 3 kV, a beam current of 200 pA, and a working distance of 8 mm (Gemini 2, Zeiss, Germany).

The electronic resistivity of the extruded granules was determined after grinding, using a four-point measurement setup (Mitsubishi Chemical Analytech, MCP-PD51, Japan). The resistivity of the samples was measured at five different compaction pressures of 12, 25, 38, 51, and 64 MPa. Each measurement was repeated three times, using fresh samples. The compressibility was simultaneously determined by measuring the thickness of the samples in the measuring cell at the various applied pressures.

The composite layer and interface resistance of the electrodes were characterized, using a Hioki RM2610 (Japan) measurement system. This system employs 46 pins to apply a constant current and measure the potential distribution across the electrode surface. The electronic composite resistivity and the interface resistivity between the FSF and the primed current collector were determined by modeling the electrode sheet and performing calculations based on measured data.

The tensile strength of the FSFs was determined to study their mechanical integrity. Therefore, the FSFs were cut into 100 mm long stripes with a width of 15 mm, and these were clamped in a universal testing machine (Z010, Zwick Roell, Germany). A pre-tensile force of 0.1 N was applied and afterwards the FSFs were pulled with a speed of 100 mm min^{-1} in calendering direction, coinciding with the fibrillation direction until tearing. Each tensile test was performed three times.

To investigate the influence of CB distribution on ionic resistance, electrodes with 12 mm diameter and comparable porosities differing by less than 1 % were matched together, assembled in symmetrical cells with one glass fiber separator (Whatman, USA) and 60 μL of blocking electrolyte. As blocking electrolyte, a 50 mM tetrabutylammonium perchlorate solution in ethyl carbonate (EC) and ethyl methyl carbonate (EMC) in a weight ratio of 3–7 was used to ensure no charge transfer between the solid/liquid interface. Electrochemical impedance spectroscopy (EIS) was performed under blocking conditions according to Landesfeind et al. [37]. All measurements were conducted at 25 °C, using a multichannel potentiostat (VMP3, Biologic, France). The frequency range spanned from 0.05 Hz to 99 kHz and a voltage amplitude of 10 mV was applied. A simplified transmission line model described in Landesfeind et al. [37] was employed to fit the measured impedance spectra. Equation (1) was used to calculate the tortuosity τ.

$$\tau = R_{ion}\, A\, \kappa\, \varepsilon \,/\, 2\, d \quad [1]$$

where, R_{ion} is the ionic resistivity, A the electrode area, κ the ionic

conductivity of the electrolyte, ε the electrode porosity, and d the electrode thickness. Since the measured impedance represents the combined impedance of both electrodes, the divisor of two is included in the equation. Three cells were assembled and measured for each sample.

2.3. Cell assembly

The electrochemical performance of the dry-coated cathodes was evaluated in SLP cells, which were assembled in dry room atmosphere with a dew point below −50 °C. The cathodes and anodes featured areas of 24.97 cm^2 and 29.13 cm^2, respectively. The areal capacities of the electrodes were balanced in a negative-to-positive (N/P) ratio of 1.1 and assembled with a commercial polyolefin separator with a thickness of 25 µm (Celgard USA), 270 µL (2.74 mL Ah^{-1}) of electrolyte, consisting of EC, EMC, dimethyl carbonate in a 1:1:1 gravimetric ratio with 1 mol L^{-1} lithium hexafluorophosphate ($LiPF_6$) and 0.2 mol L^{-1} lithium bis(fluorosulfonyl)imide (LiFSI) as conductive salts.

2.4. Formation and electrochemical characterization

The full cells were pressurized with 4.1 MPa by metal cell holders during formation and electrochemical testing. Press pads were utilized to guarantee even pressure distribution. In the cell formation, the SLP cells were charged and discharged between 2.8 and 4.2 V with a constant current (CC) at a c-rate of 0.1C, followed by a constant voltage (CV) step at 4.2 V until a threshold current corresponding to 0.05C was reached. For final electrolyte soaking, the cells were charged to 50 % State of Charge (SoC) and rested for five days at 25 °C.

The electrochemical properties of the SLP cells were characterized through continuous cycling. Therefore, the cells were subjected to a charging step with 0.5C CC and a threshold current of 0.05C CV up to 4.2 V, followed by a 0.5C CC discharge to 2.8 V. Discharge rate capability tests were performed at the beginning of cycling and every 150 cycles thereafter from fully charged cells (C/3; CCCV) and discharge C-rates of 0.05C, 0.33C, 1 C, and 2 C. The first cycle of cycling protocol after the 2 C discharge is used for the specific capacity of the 0.5C discharge rate. All tests were conducted at 25 °C.

3. Results and discussion

3.1. Powder and granule characterization

SEM images of the premixed active material and CB were recorded to study the distribution of CB depending on the mixing time. Exemplary images for the samples P2, P10, P30, and P60 are presented in Fig. 1. The SEM images show the poly- and single-crystalline morphology of the NMC 811 active material (brighter color) and the CB (darker color). Large CB agglomerates in the powder mixture with 2 min mixing time, indicated insufficient CB agglomerate break-up. In contrast, after 10 min of mixing, the large CB agglomerates were broken down into smaller agglomerates that were no longer connected to each other. Mixing for 30 min resulted in partial coating of CB on the surfaces of the active material particles, particularly the polycrystalline particles. This coating is visible in the SEM images by distinct darkening of the particle surfaces. The rougher surface of the polycrystalline particles may have facilitated the CB attachment. Only few small agglomerates are present, with a uniform distribution of the CB. Finally, 60 min of mixing led to a homogenous distribution and a complete surface coating of CB on the polycrystalline active material particles, with no visible CB agglomerates. Only small spots of the single crystalline particles are covered with CB. The SEM analysis revealed that the four mixing times produced powders with significantly different CB distributions, which will be further investigated. Importantly, no particle cracking of the active material is observable in the SEM images, excluding excessive energy input on the active material particles during mixing.

For the following analysis of the electronic resistivity and compressibility, the extruded granules with fibrillated PTFE were used as samples. Fig. 2a displays the relationship between the applied pressure and the composite density, revealing that crushing CB agglomerates by longer mixing times allows to achieve higher densities at equivalent pressure levels. Specifically, the samples G2 and G10, which contained remaining CB agglomerates, reached a maximum density of approximately 3.5 g cm^{-3}. In contrast, the samples G30 and G60 with few to no CB agglomerates and a coating of the active material achieved densities of around 3.8 g cm^{-3}. Through the break-up of the CB agglomerates and the surface coating, more open pores could be generated, whereby the compressibility increases. The facilitated compaction of composites

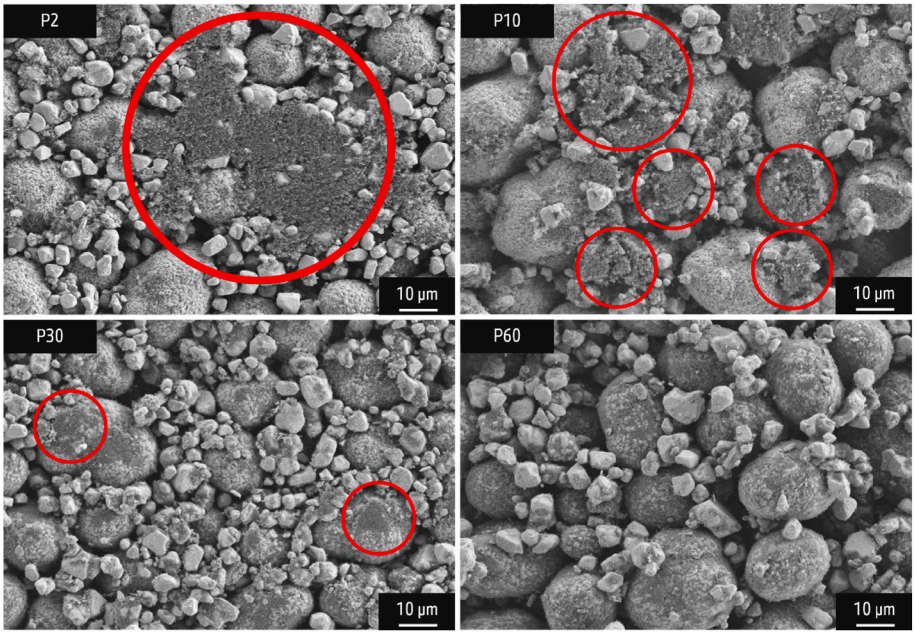

Fig. 1. SEM images of premixed powders with NMC 811 and CB after 2, 10, 30, and 60 min of mixing. Red circles highlighting exemplary CB agglomerates in the mixtures (darker contrast), which are especially present in P2 and become more deagglomerated for extended mixing times.

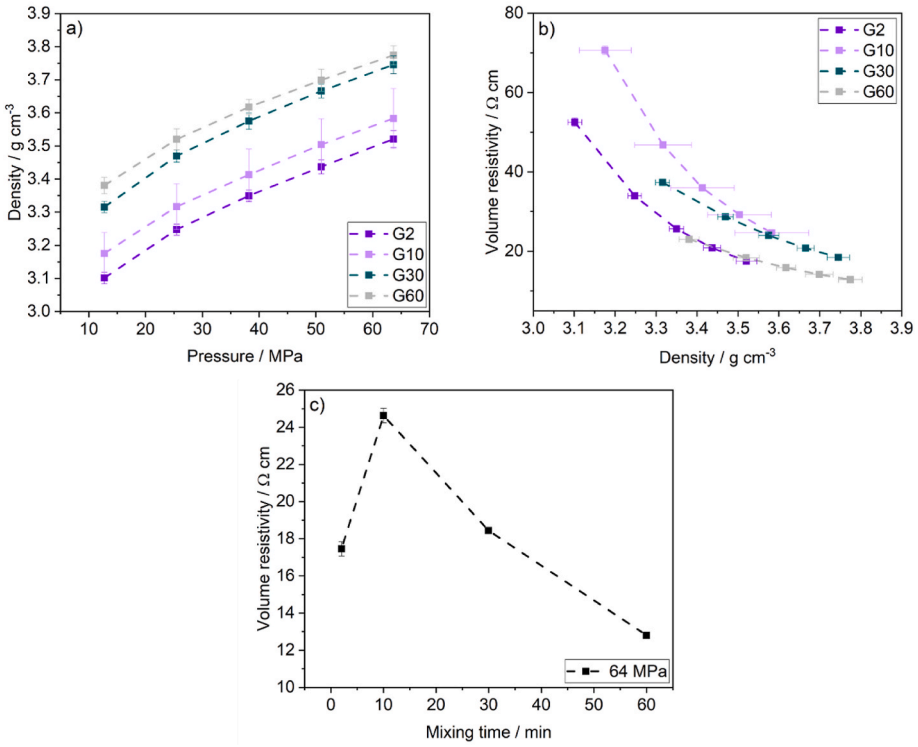

Fig. 2. Granule characterization by measuring the electronic resistivity as a function of the density. (a) Compaction behavior of composite granules, (b) correlation of resistivity and density for composite granules, (c) resistivity dependent on the mixing time at a pressure of 64 MPa for composite granules. The connecting lines between the data points serve as guide-to-the-eye.

might allow to reduce the compaction forces during calendering, mitigating particle cracking and roller damage. The electronic resistivity of the samples, as shown in Fig. 2b, correlates strongly with the density. This is in alignment with the fact that the particle contacts increase with higher density, facilitating electron transport [38]. The homogenous distribution of CB and the lack of CB agglomerates after 60 min of mixing, resulted in the highest densification and least electronic resistivity. This is also attributed to the conductive CB coating on the surface of the active material and the improved particle contact under the applied pressure. Similar applies for 30 min of mixing, whereby the resistivity increased to a level similar to the sample G2 for the same applied pressures although the density of G30 is higher. This suggests that the large CB agglomerates after 2 min of mixing can interconnect under a certain pressure and density and establish a percolation network, maintaining sufficient conductivity. However, the resistivity after 10 min of mixing increased, indicating that the small, isolated CB

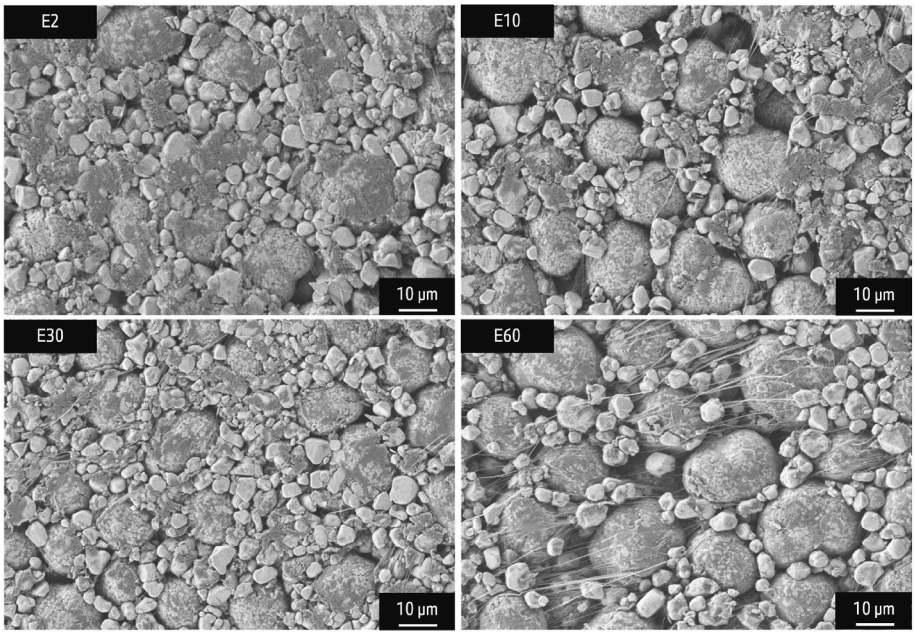

Fig. 3. Exemplary SEM images of electrode surfaces of E2, E10, E30, and E60 showing the CB distribution and the PTFE fibrils on the surface.

agglomerates are unable to form an effective percolation network, which is crucial for the electronic conductivity of CB-containing composites [20,39]. At a density of 3.5 g cm^{-3}, which corresponds to the electrode density, the resistivities of G2 and G60 were comparable, as were the resistivites of G10 and G30. Fig. 2c shows the electronic resistivity of the composite granules as a function of the mixing time at a fixed pressure of 64 MPa. Compared to 2 min of mixing, the resistivity increased from 17.5 Ω cm to 24.6 Ω cm after 10 min. This can be explained with the break-up of the CB into small agglomerates, incapable of establishing a percolation network. However, this trend reversed with the resistivity decreasing to approximately 18.4 Ω cm and 12.8 Ω cm after 30 and 60 min of mixing as the density increased and the uniform CB distribution helped to form a continuous electronic network.

3.2. Electrode characterization

SEM analyses of the surfaces of the produced electrodes (see Fig. 3) showed a similar trend for the CB distribution observed in the powder premix (see Fig. 1) on electrode level. The electrode fabricated from a premix with 2 min of mixing time, showed large CB agglomerates on the surface, while only few small CB agglomerates were present in the sample dispersed for 10 min. The electrode produced with a 30-min CB dispersion time showed a partial coating of the active material particles, with small CB agglomerates remaining. A uniform and homogenous CB coating of the active material surface was achieved for the sample based on the powder premixed for 60 min. The SEM images confirm that prolonged dispersion times of the CB lead to a more homogenous distribution of the CB in the cathode. Intensive energy input at longer mixing time resulted in a homogenous coating of the active material particles with CB. Moreover, the SEM images indicate a correlation between the CB distribution and the occurrence of PTFE fibrils and reveal that the PTFE fibrils predominantly occur in regions, where CB is present. This phenomenon was already discussed in the work of Huber et al. [40], where the SEM images also indicated affinity of the CB and the PTFE. In E2, only few small fibrils are observed co-located with CB agglomerates, with some fibrils embedded within the CB agglomerates. However, areas devoid of CB show no PTFE fibrillation. A more homogenous distribution of the CB apparently led to finer, more uniformly dispersed fibrils. This becomes particularly clear in E60, where a homogenous fibrillation of the PTFE along the calendering direction is identifiable. The fibrils are also more exposed and less enclosed by CB domains. These observations indicate that the surface of the CB promotes the PTFE fibrillation during calendering. Pull tests in the calendering direction were conducted using FSFs to examine the degree of PTFE fibrillation. The results are shown in Fig. 4.

The tensile strength of the FSFs increased from less than 0.5 N mm^{-2} to more than 0.6 N mm^{-2} for E30 and E60 compared to the electrodes E2 and E10. The higher tensile strengths correlated to longer mixing times can be attributed to an increased homogeneity of the CB. It is hypothesized that during calendering, the surface of the CB particles provide initial attachment sites for the PTFE fibrils, from where the fibers are elongated. Through a homogenous distribution of the CB, more attachment sites are available for the PTFE, whereby the amount of fibrils increases. In the case of the electrodes E30 and E60, the uniform CB distribution led to an increased available surface of the CB, correlating to more PTFE fibrils. A uniform distribution, which improves the mechanical stability of the FSFs, might allow a reduction of the binder content in the electrode formulation.

Beyond the mechanical product properties, the granules G30 and G60 possessed an increased flowability, which was observable by a facilitated intake of the powder into the calendar gap. This is in accordance with the results of Gyulai et al. [41], who already described an enhanced granule flowability for more homogenous powder mixtures. The linear loads of each calendering step are listed in Table 1. The linear load during calendering was reduced from 100 N mm^{-1} to 40 N mm^{-1} in the first step and to 30 N mm^{-1} in the second and third calendering step

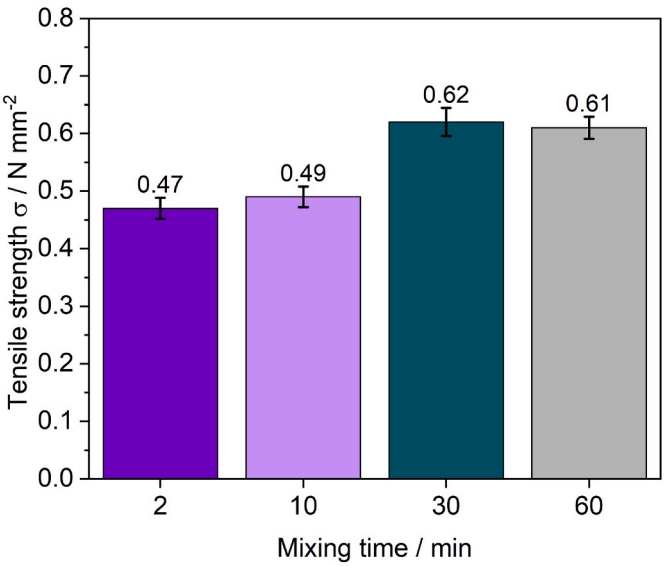

Fig. 4. Results of tensile strength tests in calendering direction of FSFs.

Table 1
Linear loads during calendering for the tested granules.

Sample	Line load 1st step/N mm^{-1}	Line load 2nd step/N mm^{-1}	Line load 3rd step/N mm^{-1}
G2	100	100	80
G10	100	100	80
G30	40	30	30
G60	40	30	30

for both samples with homogenous CB distribution. Calendering of G30 and G60 at higher linear loads was expected to lead to an overcompaction of the granules. This aligns well with the compressibility measurements of the granules in subchapter 3.1, which demonstrated easier densification of G30 and G60.

To evaluate the dependence of the electrode structure on the electronic and ionic properties of the electrodes, the resistances were determined. The composite resistivities of the electrodes are presented in Fig. 5a. The electrode E2 with large CB agglomerates, and E30 with partial coating and small CB agglomerates showed similar resistivities at around 17 Ω cm. In comparison, E10 displayed an increase in resistivity up to 23 Ω cm, likely due to the small CB agglomerates being unable to form a continuous percolation network across the electrode as described above. However, the combination of partial particle coating with small CB agglomerates in E30 proved preferable, providing both short- and long-range electronic pathways throughout the electrode [19]. The trend in electronic resistivity of E2, E10, and E30 was as expected from the granule bulk resistivity measurements in subchapter 3.1, see Fig. 2. For E60 on the contrary, the resistivity was 21 Ω cm, contrasting the behavior observed during granule characterization, where the lowest resistivity was observed for G60. While the granules achieve quasi-zero porosity under high pressures, the electrodes comprise remaining pores that reduce the particle contact. The surface coating of the active material binds the CB, leading to mostly short-range electronic paths that only insufficiently form an electronic percolation network. In addition, SEM analyses revealed pronounced occurrence of PTFE fibrils on the surface of E60. This electronic inactive compound on the surface of the electrode promotes the increase of the electronic resistance. Nevertheless, in consideration of the standard deviations, the differences in the electronic resistivity are considerably small. The interface resistances between the FSF and the current collector are shown in Fig. 5b. Particularly interesting is the increased resistivity of E60 of 0.07 Ω cm^2 compared to all other samples which displayed similar, lower values of

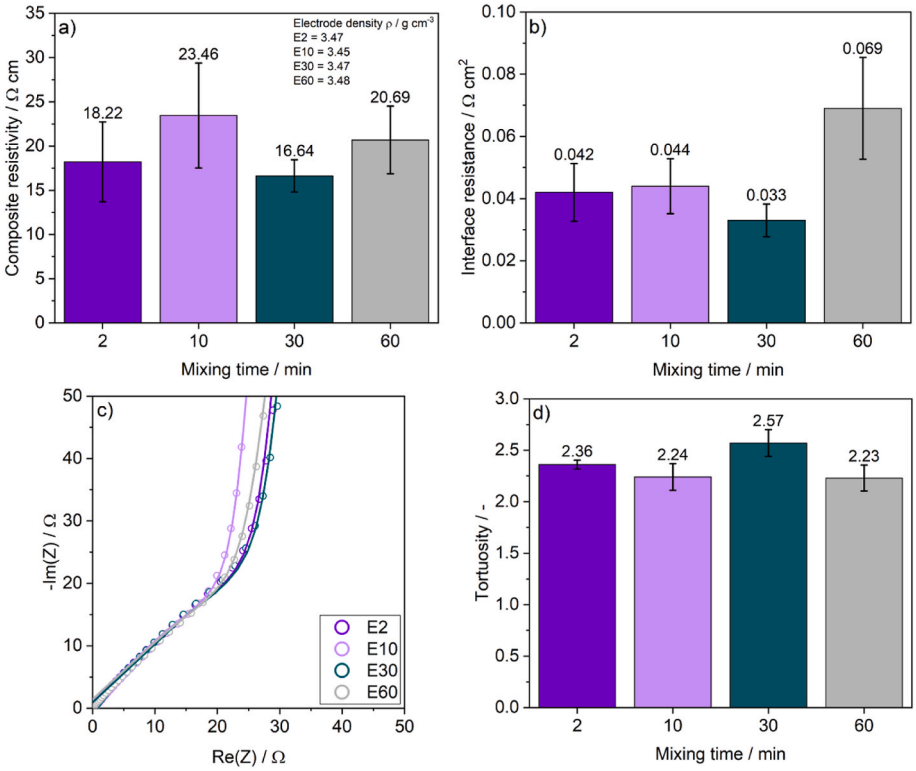

Fig. 5. Electronic resistances and tortuosities of manufactured dry electrodes; (a) composite resistivity of the electrodes, (b) interfacial resistance between FSF and current collector, (c) exemplary Nyquist-Plot of impedance measurement under blocking conditions with fits from transmission line model, (d) tortuosity values for electrodes determined from transmission line model.

around 0.04 Ω cm^2. The elevated resistance suggests that the distribution of CB has a minor effect on the interfacial resistivity. The increased interfacial resistivity observed for electrode E60 might originate from the extensive fibrillation of the PTFE on the surface of the electrode (see Fig. 3), which is laminated onto the current collector. The large quantity of the non-conductive PTFE likely contributed to an overall increase in the electronic resistivity between the FSF and the current collector.

In Fig. 5c, one exemplary Nyquist plot of each sample is shown together with the transmission line model fit [37]. The plots exhibit a linear 45° increase, which indicates a diffusion-controlled process. A steep increase in the curve signifies limited diffusion and the onset of capacitive behavior. Notably, the Nyquist plots exhibit only small differences, suggesting a minor impact of the CB distribution on the ionic resistance within the electrode. The onset for capacitive behavior is slightly shifted towards lower resistances for electrodes E10 and E60. Calculation of the tortuosity using equation [1] revealed similar values for E2, E10, and E60, all within the standard deviation as depicted in Fig. 5d. The tortuosity appeared to decrease with a more homogenous CB distribution, potentially due to the absence of CB agglomerates that could obstruct the Li^+ transport pathways [42]. Only E30 showed slightly increased tortuosity. The higher number of fibrils on the surfaces of E30 and E60 could cause an increase in the tortuosity, whereby the effects of CB distribution and PTFE fibrillation cancel each other out. The interplay between the CB distribution and the PTFE affects the overall electrode properties.

3.3. Electrochemical characterization

The electrodes were assembled to SLP cells to study the effect of the CB distribution on the electrochemical characteristics of the dry-coated cathodes. The respective electrode characteristics and the most relevant data gained from the formation cycle are summarized in Table 2. The different cells reached comparable first-cycle coulombic efficiencies of approximately 90 % and a comparable specific discharge capacity of around 209 mA h g^{-1}.

Table 2
Electrode characteristics and formation cycle data of SLP cells.

Electrode	Areal Capacity/ mAh cm^{-2}	Electrode density/g cm^{-3}	Coulombic Efficiency/%	$Q_{discharge}$/mAh g_{NMC}^{-1}
E2	4.05	3.47	90.45 ± 0.27	209.05 ± 0.88
E10	3.92	3.45	90.86 ± 0.21	209.73 ± 0.48
E30	3.99	3.47	90.64 ± 0.20	209.19 ± 0.34
E60	4.06	3.48	90.78 ± 0.30	209.79 ± 0.11

The electrochemical cell testing results are displayed in Fig. 6. In the cycling stability test (Fig. 6a), capacity retentions of approximately 91 % were obtained for E2, E30, and E60 after 600 cycles, whereas an increased capacity fade was observed for E10 after 300 cycles, resulting in a capacity retention of 87 % after 600 cycles. The comparable cycling performance of the cells containing the electrodes E2, E30, and E60 can be attributed to their analogous electronic resistance and tortuosity, as detailed in subchapter 3.2 (see Fig. 5). Notably, E60 experienced accelerated capacity loss during the initial cycles. After the first 10–15 cycles, the curve flattened, aligning with the course of the other cells. The accelerated capacity loss indicates an increase in resistance and overpotential in these cells when subjected to higher discharge currents. This phenomenon could be caused by the CB coating on the surface of the active material, which potentially restricts Li-ion diffusion into the active material, thereby increasing overpotential [29]. As the electrode reached equilibrium following the initial cycles, the overpotential decreased. Despite these differences, the overall cycling performance of the electrodes E2, E30, and E60, when accounting for the standard deviation of the cycling data, was found to be similar. The diminished cycling stability of E10 can be attributed to its inferior electronic

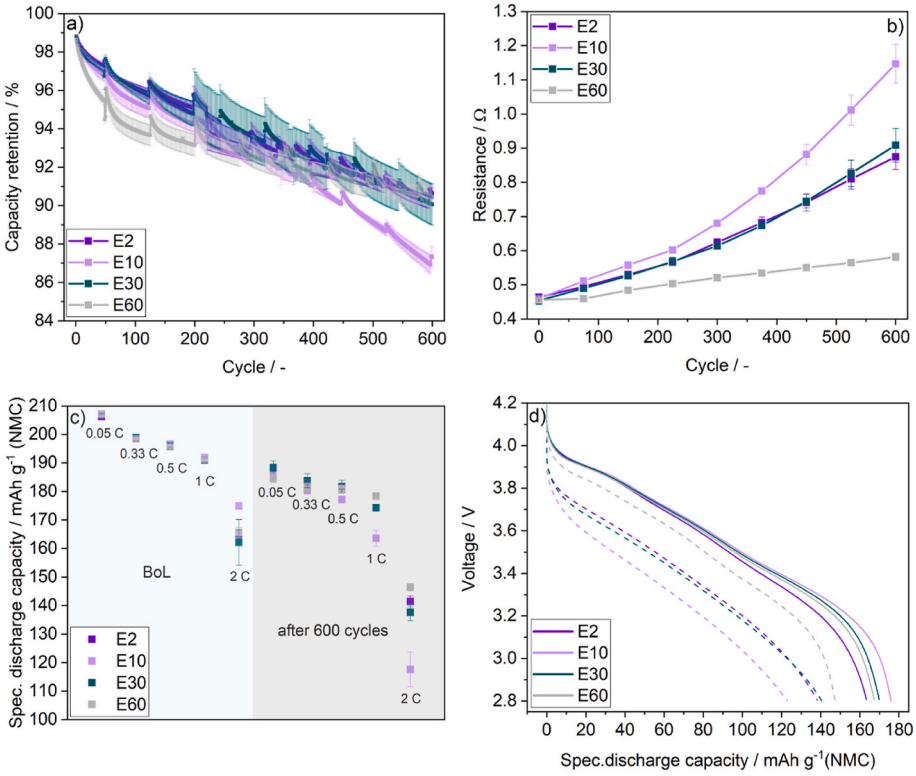

Fig. 6. Results from electrochemical testing; (a) cycle life over 600 cycles at C/2, (b) DCIR tests at 80 % SOC after 1 s, (c) rate discharge tests at BoL and after 600 cycles at 0.05C, 0.33C, 0.5C, 1 C, and 2 C, (d) potential curves of 2 C rate discharge tests at BoL (solid line) and after 600 cycles (dashed line).

properties, as characterized in subchapter 3.1 and 3.2. The intermediate mixing time of 10 min resulted in the formation of small CB agglomerates, which potentially could not establish a sufficient percolation network. The findings from the direct current internal resistance (DCIR) tests after 1 s at 80 % state of charge (SOC) support this hypothesis (see Fig. 6b). The internal resistance of the cells containing the electrode E10 exhibited a significant increase after 300 cycles, ultimately doubling in comparison to the cells with E60 after 600 cycles. In contrast, the electrodes E2 and E30 displayed a comparable course of resistance during cycling, with values between those of E10 and E60. After 1 s, the time corresponding to our measurement conditions, the ohmic and electronic as well as the charge transfer resistances dominate [43–46]. Consequently, the resistance values in Fig. 6b indicate that the uniform distribution of the CB in E60 is beneficial for the electronic properties of the electrode. The discharge rate capability, illustrated in Fig. 6c, revealed negligible differences at begin of life (BoL) for discharge rates up to 1C. At a 2C discharge rate, the electrode E10 reached a specific discharge capacity of 174.92 mAh g^{-1}, surpassing the other samples by approximately 10 mAh g^{-1}. This enhanced rate capability might result from the slightly lower ionic resistance and tortuosity of the electrode E10 (see Fig. 5). After 600 cycles, the discharge capacities at 0.05C and 0.33C were similar for all electrodes as well. At discharge rates of 1 C and 2 C, however, the capacities of E10 demonstrated.

Capacities that were 10 mA h g^{-1} and 20 mA h g^{-1} lower, respectively, than those of E2 and E30, which exhibited similar rate capabilities. The discrepancy is in alignment with the increased internal resistance observed in cells with E10 during cycling, contributing to accelerated degradation. This is also confirmed by the potential curve at of E10 at 2 C (see Fig. 6d, dashed lines), which shows an increased overpotential after 600 cycles. In contrast, cells incorporating E60 reached discharge capacities that were 5 mA h g^{-1} higher than E2 and E30 at high discharge rates of 1 C and 2 C. This finding is consistent with the cycling test results and the constantly low DCIR throughout the cycle life. Also, the potential curves after 600 cycles shown in Fig. 6d, demonstrate only slightly increased overpotential at 2 C for the cells from E60 in contrast to the cells containing E2 and E30.

The electrochemical performance of E2 and E30 exhibited comparable cycling and rate capability, attributed to their similar electrode properties. Conversely, the electrochemical performance of E10 was adversely affected by its inferior electronic properties, leading to an increased DCIR and accelerated capacity fade. The cycling stability of E60 was comparable to that of E2 and E30. However, the rate capability of E60 after 600 cycles at high discharge rates was notably superior. The findings underscore the critical importance of establishing a sufficient percolation network of the CB within the electrode structure. The observed beneficial effect of uniform CB distribution is further corroborated by findings reported in existing literature [24,25,29,30], which emphasizes the necessity of both short- and long-range electronic contacts within the conductive carbon network. However, if a sufficient percolation network is established within the electrode, the electronic properties do not limit the overall electrochemical performance. The importance of a uniform CB distribution increases for electrode formulations with lower shares of CB.

3.4. *Optimizing electrode formulation*

The results from the electrochemical characterization demonstrated that, when a sufficient percolation network is achieved, variations in CB distribution, as observed in E2 and E60, can lead to similar electrochemical performances. However, the results from the electrode characterization presented in subchapter 3.2 indicated that a more uniform CB distribution contributes to a more homogenous and stronger fibrillation of the PTFE (see Fig. 3) and to a higher tensile strength, which was quantitatively assessed through tensile strength tests of the FSFs. Based

on these findings, attempts were made to reduce the PTFE content from 1 wt% to 0.8 wt% and 0.6 wt% in the composites G2 and G60 to increase the active material share. It was possible to produce FSFs with 0.8 wt% and 0.6 wt% PTFE from the composite that underwent 60 min of premixing of the active material and CB. However, with 2 min of mixing, only FSFs with 0.8 wt% PTFE could be successfully processed from the composite, while the formulation with 0.6 wt% PTFE shows instability and fissuring of the FSF, see S1. In Fig. 7, the results of the tensile strength tests of the FSFs with reduced binder content are shown.

The reduction of the binder content from 1 wt% to 0.8 wt% for the composite, which was mixed for 2 min resulted in a significant reduction in tensile strength from 0.47 N mm^{-2} to 0.22 N mm^{-2}, leading to increased brittleness of the FSFs and processing difficulties. Conversely, for G60, when the CB was uniformly distributed, a similar reduction in binder content from 1 wt% to 0.8 wt% caused a decrease in tensile strength from 0.61 N mm^{-2} to 0.44 N mm^{-2}, which is comparable to the tensile strength observed for G2 with 1 wt% binder content. These results demonstrate that a uniform distribution of the CB facilitates enhanced fibrillation of PTFE, thereby allowing for a reduction in binder content without compromising structural integrity. Notably, even a further reduction of the binder content to 0.6 wt% in G60 yielded processable FSFs with a tensile strength of 0.31 N mm^{-2}, indicating the potential of CB distribution for optimizing binder contents in electrode formulations.

The sample G2 with 0.8 wt% binder was not processable to an electrode. Fig. 8 shows the capacity retention over 600 cycles for the samples with 0.8 wt% and 0.6 wt% PTFE from E60 in comparison to E2 and E60 with 1 wt% PTFE.

All samples exhibited a capacity retention of 91 % after 600 cycles, demonstrating no significant differences during aging tests and degrading similarly to the cycle life of the cells depicted in Fig. 6a. These findings support the hypothesis that varying CB distributions, as in E2 and E60, can yield comparable capacity retentions. A more detailed analysis of these cells falls outside the scope of this study.

Overall, the results presented in this section indicate that the binder content can be reduced by 40 % in the electrode formulation through homogenous distribution of the CB in the electrode. This reduction allows for an increase in the active material content, leading to higher energy densities in the cell. This effect is particularly pronounced when

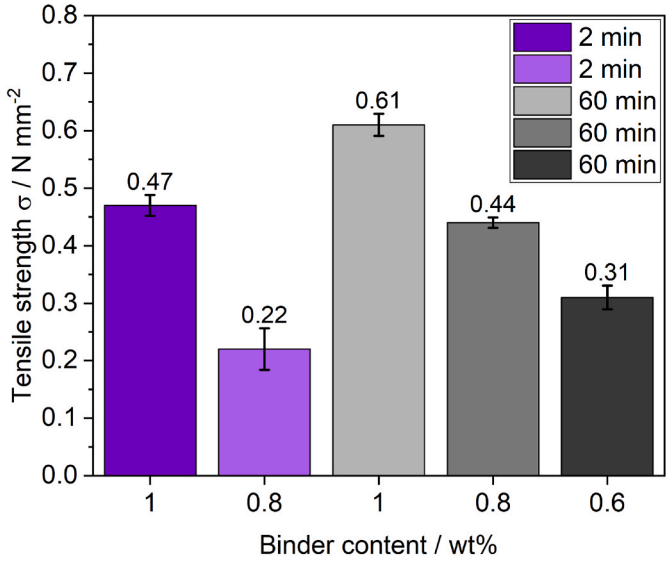

Fig. 7. Results of tensile strength tests in calendering direction of FSFs with reduced binder content for two and 60 min of premixing of active material and CB in comparison to the base recipe with 1 wt% PTFE.

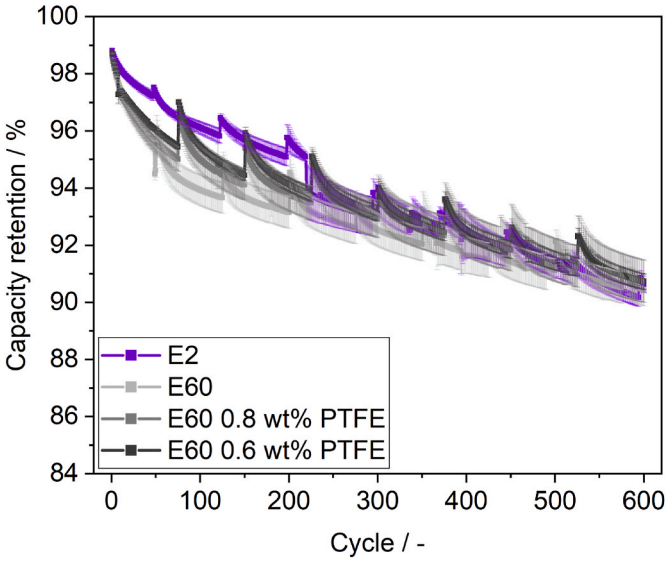

Fig. 8. Capacity retention over 600 cycles at C/2 for E2, E60, and E60 with reduced binder contents of 0.8 wt% and 0.6 wt% PTFE. Tests were performed in SLP cells accordingly to the cell tests in subchapter 3.3.

applied to large format cells, suggesting significant potential for optimizing electrode formulations in energy storage application.

4. Conclusion

In this work, the influence of CB distribution on the calendering step during dry coating and on the mechanical and electronic properties of the yielded cathodes was studied. Varying the premixing time of the cathode active material with the CB showed a feasible lever to control the CB distribution in the intermediate products and the final electrode. Among the investigated mixing times of two, ten, 30, and 60 min, extended mixing durations facilitated enhanced deagglomeration of CB, resulting in a more uniform CB distribution and effective surface coating of cathode active material particles. SEM images demonstrated that deagglomeration of CB was observable after 10 min of mixing, while surface coating of the active material particles became apparent after 30 min. After 60 min, no CB agglomerates were visible. The composite granules were further characterized in terms of compressibility, electronic resistance, and microstructure. The obtained composites were processed to electrodes in a multi-step calendering process.

A more homogenous distribution of the CB resulted in improved granule compressibility, allowing for a reduction of the linear load during calendering by 60–70 % for the samples premixed for 30 and 60 min. The mechanical, electronic, ionic and the electrochemical characteristics of the electrodes were systematically analyzed with a specific focus on the interplay between CB distribution and the fibrillation of the PTFE binder. SEM images showed that a more homogenous CB distribution significantly improved the extent and homogeneity of PTFE fibrillation, leading to higher tensile strengths for FSFs on the basis of granules prepared from active material and CB that were premixed for 30 and 60 min. An electrode yielded from a composite, which was premixed for 10 min, with small CB agglomerates showed inferior electronic properties due to an insufficient electronic percolation network resulting from suboptimal CB distribution. Additionally, an increased interface resistance was detected for the sample mixed for 60 min with a uniform CB distribution, attributed to the isolating effects of the fibrils, which were more distinct at the interface between the coating and the current collector in this electrode. The electrodes yielded from the composites, which underwent two and 30 min of premixing showed similar electronic properties. The minimal influence of the CB distribution on the ionic resistance was traced back to counteracting effects

on the CB distribution and PTFE fibrillation. Inferior electronic properties of an electrode processed from the composite with a premix of active material and CB for 10 min, corresponded with the poorest electrochemical performance, while all other samples exhibited comparable electrochemical performances. However, the electrode yielded from the composite, which underwent 60 min of premixing with uniform CB distribution, ensured a consistently low internal resistance. It was further shown that the binder content could be reduced by 40 % for the formulation, where the CB was uniformly distributed after 60 min compared to the formulation, which was premixed for 2 min due to the higher extent of PTFE fibrillation.

This work gives clear evidence on how more homogenous CB distributions positively influenced both the calendering step and the PTFE fibrillation. Better compressibility of the granules facilitated a reduction in the required calendering forces. Resulting from a uniform CB distribution, an enhanced PTFE fibrillation was detected, which might diminish the risks of web breaks and enables the opportunity to reduce the binder content in the electrode, potentially enhancing overall electrode performance. A homogeneous CB distribution characterized by a sufficient percolation network is essential for optimal electrochemical performance. The results contribute to advancements in the fabrication of dry-coated cathodes and optimizing mixing protocols and electrode formulations, tailored to every manufacturing process individually. The findings could also be implemented in simulation models that incorporate the effect of CB distribution. The incorporation of carbon nanotubes (CNTs) with CB should be the focus of further investigations to establish long-range electronic contacts in electrodes, where CB is coated on the cathode active material surface to improve processibility.

CRediT authorship contribution statement

Serkan Z. Damnali: Writing – original draft, Visualization, Methodology, Investigation, Formal analysis, Conceptualization. **Benjamin Villard:** Writing – review & editing, Methodology, Investigation, Data curation. **Matthias Leeb:** Writing – review & editing, Methodology, Conceptualization. **Berkant Tekin:** Writing – review & editing, Methodology, Investigation. **Thomas Woehrle:** Writing – review & editing, Conceptualization. **Ruediger Daub:** Writing – review & editing. **Alice Hoffmann:** Writing – review & editing, Validation. **Markus Hoelzle:** Writing – review & editing, Supervision.

Declaration of competing interest

The authors declare the following financial interests/personal relationships which may be considered as potential competing interests: Serkan Z. Damnali reports financial support was provided by BMW Group. Benjamin Villard reports financial support was provided by BMW Group. Berkant Tekin reports financial support was provided by BMW Group. Thomas Woehrle reports financial support was provided by BMW Group. Serkan Z. Damnali reports a relationship with BMW Group that includes: employment. Benjamin Villard reports a relationship with BMW Group that includes: employment. Berkant Tekin reports a relationship with BMW Group that includes: employment. Thomas Woehrle reports a relationship with BMW Group that includes: employment. If there are other authors, they declare that they have no known competing financial interests or personal relationships that could have appeared to influence the work reported in this paper.

Acknowledgements

This work was funded by the BMW Group within its ProMotion Program. The autors wish thank to the German Federal Ministry for Economic Affairs and Energy and the Bavarian Ministry of Economic Affairs, Regional Development and Energy for funding this work in the project “IPCEI II EuBatIn (16BZF205)”. The authors wish also thank to Cabot Corporation (USA) for providing the carbon black used in this work and Chemours (USA) for providing the PTFE used in this work.

Appendix A. Supplementary data

Supplementary data to this article can be found online at https://doi.org/10.1016/j.jpowsour.2025.238924.

Data availability

The authors do not have permission to share data.

References

[1] Y. Lu, C.-Z. Zhao, H. Yuan, J.-K. Hu, J.-Q. Huang, Q. Zhang, Dry electrode technology, the rising star in solid-state battery industrialization, Matter 5 (2022) 876–898, https://doi.org/10.1016/j.matt.2022.01.011.
[2] Y. Li, Y. Wu, Z. Wang, J. Xu, T. Ma, L. Chen, H. Li, F. Wu, Progress in solvent-free dry-film technology for batteries and supercapacitors, Mater. Today 55 (2022) 92–109, https://doi.org/10.1016/j.mattod.2022.04.008.
[3] W. Jin, G. Song, J. Yoo, S. Jung, T. Kim, J. Kim, Advancements in dry electrode technologies: towards sustainable and efficient battery manufacturing, Chemelectrochem 11 (2024) e202400288, https://doi.org/10.1002/celc.202400288.
[4] D. Liu, L.-C. Chen, T.-J. Liu, T. Fan, E.-Y. Tsou, C. Tiu, An effective mixing for lithium ion battery slurries, Adv. Chem. Eng. Sci. 4 (2014) 515–528, https://doi.org/10.4236/aces.2014.44053.
[5] B. Ludwig, Z. Zheng, W. Shou, Y. Wang, H. Pan, Solvent-free manufacturing of electrodes for lithium-ion batteries, Sci. Rep. 6 (2016) 23150, https://doi.org/10.1038/srep23150.
[6] R. Sliz, J. Valikangas, H. Silva Santos, P. Vilmi, L. Rieppo, T. Hu, U. Lassi, T. Fabritius, Suitable cathode NMP replacement for efficient sustainable printed Li-Ion batteries, ACS Appl. Energy Mater. 5 (2022) 4047–4058, https://doi.org/10.1021/acsaem.1c02923.
[7] N. Susarla, S. Ahmed, D.W. Dees, Modeling and analysis of solvent removal during Li-ion battery electrode drying, J. Power Sources 378 (2018) 660–670, https://doi.org/10.1016/j.jpowsour.2018.01.007.
[8] D. Bresser, D. Buchholz, A. Moretti, A. Varzi, S. Passerini, Alternative binders for sustainable electrochemical energy storage – the transition to aqueous electrode processing and bio-derived polymers, Energy Environ. Sci. 11 (2018) 3096–3127, https://doi.org/10.1039/C8EE00640G.
[9] M. Wang, X. Dong, I.C. Escobar, Y.-T. Cheng, Lithium ion battery electrodes made using dimethyl sulfoxide (DMSO)—A green solvent, ACS Sustain. Chem. Eng. 8 (2020) 11046–11051, https://doi.org/10.1021/acssuschemeng.0c02884.
[10] D.L. Wood, J. Li, C. Daniel, Prospects for reducing the processing cost of lithium ion batteries, J. Power Sources 275 (2015) 234–242, https://doi.org/10.1016/j.jpowsour.2014.11.019.
[11] F. Degen, O. Krätzig, Future in battery production: an extensive benchmarking of novel production technologies as guidance for decision making in engineering, IEEE Trans. Eng. Manag. 71 (2024) 1038–1056, https://doi.org/10.1109/TEM.2022.3144882.
[12] N. Golovanov, A. Marinescu, Electromobility and climate change, in: 2019 8th Int. Conf. Mod. Power Syst. MPS, IEEE, Cluj-Napoca, 2019, pp. 1–5, https://doi.org/10.1109/MPS.2019.8759786. Cluj, Romania.
[13] McKinsey & Company, Battery 2030: resilient, sustainable, and circular. https://www.mckinsey.com/industries/automotive-and-assembly/our-insights/battery-2030-resilient-sustainable-and-circular#/, 2023.
[14] B. Schumm, S. Kaskel, Dry battery electrode processing, what’s next? Energy 1 (2023) 100009 https://doi.org/10.1016/j.nxener.2023.100009.
[15] L. Zhong, X. Xi, P. Mitchell, B. Zou, Dry Particle Based Capacitor and Methods of Making Same, US007352558B2, n.d..
[16] K.J. Bigham, Drawn Fiber Polymers: Chemical and Mechanical Features, Bd. Zeus Industrial Products Technical Paper, 2018.
[17] C.J. Drummond, G. Georgaklis, D.Y.C. Chan, Fluorocarbons: surface Free Energies and van der Waals Interaction, Langmuir 12 (1996) 2617–2621, https://doi.org/10.1021/la951020v.
[18] R. Tao, Y. Gu, Z. Du, X. Lyu, J. Li, Advanced electrode processing for lithium-ion battery manufacturing, Nat. Rev. Clean Technol. 1 (2025) 116–131, https://doi.org/10.1038/s44359-024-00018-w.
[19] J. Entwistle, R. Ge, K. Pardikar, R. Smith, D. Cumming, Carbon binder domain networks and electrical conductivity in lithium-ion battery electrodes: a critical review, Renew. Sustain. Energy Rev. 166 (2022) 112624, https://doi.org/10.1016/j.rser.2022.112624.
[20] J.F. Baumgärtner, K.V. Kravchyk, M.V. Kovalenko, Navigating the carbon maze: a roadmap to effective carbon conductive networks for lithium-ion batteries, Adv. Energy Mater. (2024) 2400499, https://doi.org/10.1002/aenm.202400499.
[21] M. Prasad, S. Hein, T. Danner, B. Prifling, R. Scurtu, A. Hoffmann, A. Hilger, M. Osenberg, I. Manke, M. Wohlfahrt-Mehrens, V. Schmidt, A. Latz, Influence of conductive additives and binder on the impedance of lithium-ion battery electrodes: effect of an inhomogeneous distribution, J. Electrochem. Soc. 171 (2024) 100518, https://doi.org/10.1149/1945-7111/ad81b9.

[22] H. Bockholt, W. Haselrieder, A. Kwade, Intensive dry and wet mixing influencing the structural and electrochemical properties of secondary lithium-ion battery cathodes, ECS Trans. 50 (2013) 25–35, https://doi.org/10.1149/05026.0025ecst.
[23] J.K. Mayer, L. Almar, E. Asylbekov, W. Haselrieder, A. Kwade, A. Weber, H. Nirschl, Influence of the carbon black dispersing process on the microstructure and performance of li-ion battery cathodes, Energy Technol. 8 (2020) 1900161, https://doi.org/10.1002/ente.201900161.
[24] W. Bauer, D. Nötzel, V. Wenzel, H. Nirschl, Influence of dry mixing and distribution of conductive additives in cathodes for lithium ion batteries, J. Power Sources 288 (2015) 359–367, https://doi.org/10.1016/j.jpowsour.2015.04.081.
[25] H. Bockholt, W. Haselrieder, A. Kwade, Intensive powder mixing for dry dispersing of carbon black and its relevance for lithium-ion battery cathodes, Powder Technol. 297 (2016) 266–274, https://doi.org/10.1016/j.powtec.2016.04.011.
[26] M. Wang, D. Dang, A. Meyer, R. Arsenault, Y.-T. Cheng, Effects of the mixing sequence on making lithium ion battery electrodes, J. Electrochem. Soc. 167 (2020) 100518, https://doi.org/10.1149/1945-7111/ab95c6.
[27] C. Lischka, S. Gerl, J. Kappes, A. Chauhan, H. Nirschl, Experimental & simulative assessment of mixing quality for dry Li-Ion cathode production in an Eirich intensive mixer, Powder Technol. 431 (2024) 119072, https://doi.org/10.1016/j.powtec.2023.119072.
[28] C.Y. Lim, G. Park, K.J. Lee, Effect of carbon conductor dispersion and composition in dry cathode electrode on LiB performances, Carbon Lett. (2024), https://doi.org/10.1007/s42823-024-00812-3.
[29] A. Yonaga, S. Kawauchi, Y. Mori, L. Xuanchen, S. Ishikawa, K. Nunoshita, G. Inoue, T. Matsunaga, Effects of dry powder mixing on electrochemical performance of lithium-ion battery electrode using solvent-free dry forming process, J. Power Sources 581 (2023) 233466, https://doi.org/10.1016/j.jpowsour.2023.233466.
[30] Z. Gao, J. Fu, C. Podder, X. Gong, Y. Wang, H. Pan, Particle interactions during dry powder mixing and their effect on solvent-free manufactured electrode properties, J. Energy Storage 83 (2024) 110605, https://doi.org/10.1016/j.est.2024.110605.
[31] H. Choi, D. Moon, J. Sheem, J.K. Koo, S. Hong, S.-M. Oh, Y.-J. Kim, A solvent-free process enabled by polytetrafluoroethlyene/carbon black composites for fabricating electrodes for lithium-ion batteries with a high volumetric energy, J. Electrochem. Soc. 170 (2023) 090511, https://doi.org/10.1149/1945-7111/acf525.
[32] H. Oh, G.-S. Kim, B.U. Hwang, J. Bang, J. Kim, K.-M. Jeong, Development of a feasible and scalable manufacturing method for PTFE-based solvent-free lithium-ion battery electrodes, Chem. Eng. J. 491 (2024) 151957, https://doi.org/10.1016/j.cej.2024.151957.
[33] M. Horst, F. Beverborg, L. Bahlmann, S. Schreiber, J. Gerk, P. Michalowski, A. Kwade, Effect of active material morphology on PTFE-fibrillation, powder characteristics and electrode properties in dry electrode coating processes, Powder Technol. 451 (2025) 120451, https://doi.org/10.1016/j.powtec.2024.120451.
[34] R. Tao, B. Steinhoff, C.H. Sawicki, J. Sharma, K. Sardo, A. Bishtawi, T. Gibbs, J. Li, Unraveling the impact of the degree of dry mixing on dry-processed lithium-ion battery electrodes, J. Power Sources 580 (2023) 233379, https://doi.org/10.1016/j.jpowsour.2023.233379.
[35] H. Oh, G.-S. Kim, J. Bang, S. Kim, K.-M. Jeong, Dry-processed thick electrode design with a porous conductive agent enabling 20 mA h Cm $^{-2}$ for high-energy-density lithium-ion batteries, Energy Environ. Sci. 18 (2025) 645–658, https://doi.org/10.1039/D4EE04106B.
[36] S.Z. Damnali, K. Mazloumi, B. Tekin, T. Woehrle, A. Hoffmann, M. Hoelzle, Effect of carbon black properties on dry electrode processing of cathodes for lithium-ion batteries, J. Power Sources 646 (2025) 237243, https://doi.org/10.1016/j.jpowsour.2025.237243.
[37] J. Landesfeind, J. Hattendorff, A. Ehrl, W.A. Wall, H.A. Gasteiger, Tortuosity determination of battery electrodes and separators by Impedance spectroscopy, J. Electrochem. Soc. 163 (2016) A1373–A1387, https://doi.org/10.1149/2.1141607jes.
[38] J. Sánchez-González, A. Macías-García, M.F. Alexandre-Franco, V. Gómez-Serrano, Electrical conductivity of carbon blacks under compression, Carbon 43 (2005) 741–747, https://doi.org/10.1016/j.carbon.2004.10.045.
[39] I. Balberg, A comprehensive picture of the electrical phenomena in carbon black–polymer composites, Carbon 40 (2002) 139–143, https://doi.org/10.1016/S0008-6223(01)00164-6.
[40] K. Huber, S. Stojcevic, Y.-C. Hsieh, E.B. Müftügil, J. Terada, C. Schriever, A. Kwade, Dry battery electrode production enabled by a scalable, continuous powder mixing, J. Energy Storage 124 (2025) 116850, https://doi.org/10.1016/j.est.2025.116850.
[41] A. Gyulai, W. Bauer, H. Ehrenberg, Dry electrode manufacturing in a calendar: the role of powder premixing for electrode quality and electrochemical performance, ACS Appl. Energy Mater. 6 (2023) 5122–5134, https://doi.org/10.1021/acsaem.2c03755.
[42] Y. Itou, N. Ogihara, S. Kawauchi, Role of conductive carbon in porous Li-Ion battery electrodes revealed by electrochemical impedance spectroscopy using a symmetric cell, J. Phys. Chem. C 124 (2020) 5559–5564, https://doi.org/10.1021/acs.jpcc.9b11929.
[43] K. Uddin, A. Picarelli, C. Lyness, N. Taylor, J. Marco, An acausal Li-Ion battery pack model for automotive applications, Energies 7 (2014) 5675–5700, https://doi.org/10.3390/en7095675.
[44] W. Waag, S. Käbitz, D.U. Sauer, Experimental investigation of the lithium-ion battery impedance characteristic at various conditions and aging states and its influence on the application, Appl. Energy 102 (2013) 885–897, https://doi.org/10.1016/j.apenergy.2012.09.030.
[45] X. Hu, S. Li, H. Peng, A comparative study of equivalent circuit models for Li-ion batteries, J. Power Sources 198 (2012) 359–367, https://doi.org/10.1016/j.jpowsour.2011.10.013.
[46] A. Barai, K. Uddin, W.D. Widanage, A. McGordon, P. Jennings, A study of the influence of measurement timescale on internal resistance characterisation methodologies for lithium-ion cells, Sci. Rep. 8 (2018) 21, https://doi.org/10.1038/s41598-017-18424-5.